# Precise laser-induced local modification of AZO:Ag films and their optical properties

Maksim M Sergeev, Vladislav R Gresko, Yaroslava M Andreeva, Lilia A Sokura, Elena V Shirshneva-Vaschenko, Tatiana E Itina, Georgii V Varygin

▶ **To cite this version:**

Maksim M Sergeev, Vladislav R Gresko, Yaroslava M Andreeva, Lilia A Sokura, Elena V Shirshneva-Vaschenko, et al.. Precise laser-induced local modification of AZO:Ag films and their optical properties. Optics and Laser Technology, 2022, 151, pp.108059. 10.1016/j.optlastec.2022.108059 . ujm-03817575v2

**HAL Id: ujm-03817575**
**https://ujm.hal.science/ujm-03817575v2**

Submitted on 18 Oct 2022

**HAL** is a multi-disciplinary open access archive for the deposit and dissemination of scientific research documents, whether they are published or not. The documents may come from teaching and research institutions in France or abroad, or from public or private research centers.

L'archive ouverte pluridisciplinaire **HAL**, est destinée au dépôt et à la diffusion de documents scientifiques de niveau recherche, publiés ou non, émanant des établissements d'enseignement et de recherche français ou étrangers, des laboratoires publics ou privés.

# Precise laser-induced below bandgap local modification of AZO:Ag films and their electrooptical properties

Maksim M. Sergeev[a], Vladislav R. Gresko[a*], Yaroslava M. Andreeva[a], Lilia A. Sokura[b], Elena V. Shirshneva-Vaschenko[c], Tatiana E. Itina[d], Georgii V. Varygin[e]

[a] Faculty of Laser Photonics and Optoelectronics, ITMO University, 197101 St. Petersburg, Russia
[b] Institute of Advanced Data Transfer Systems, ITMO University, 197101 St. Petersburg, Russia
[c] College of Optics and Photonics, CREOL, University of Central Florida 4304 Scorpius Street, Orlando, Florida 32816, USA
[d] Laboratoire Hubert Curien, UMR CNRS 5516/UJM/Univ. Lyon, Bat. F, 18 rue du Pr. Benoit Lauras, 42000 Saint-Etienne, France
[e] St. Petersburg State University, 7/9 Universitetskaya nab, St. Petersburg, Russia 199034
* Correspondence author: gresko.97@mail.ru.

**Abstract**:

The paper presents precise modifications of ZnO:Al thin films with silver nanoparticles by CW laser leading to the improvement of the composite structure and optical properties. The violet laser wavelength (405 nm) was chosen to be far from the plasmon resonance wavelength. The morphology of the obtained ZnO:Al thin films with silver nanoparticles was investigated. It was detected that under an exposure by laser power densities $I_0$ = 0.89 MW/cm$^2$ and $I_0$ = 1.07 MW/cm$^2$ and scanning velocities $V_{sc}$ = 100 μm/s and $V_{sc}$ = 50 μm/s, the film structure became denser, the size of ZnO:Al crystallites increased, and the size of silver nanoparticles decreased. The effects of laser radiation on the optical characteristics of the samples were then investigated. Particularly, a blue shift of the plasmon resonance peak and an increase in the bandgap from 3.27 eV to 3.36 eV were obtained. Additionally, numerical modeling was performed based on a photothermal film processing mechanism and clearly explained the observed effects.

**Keywords:** sol-gel composites; ZnO:Al thin films; laser influence; plasmon resonance; Ag nanoparticles.

## 1. Introduction

The low cost of aluminum-doped zinc oxide, AZO (ZnO:Al), as compared to indium-tin oxide (ITO) and fluorine-doped tin oxide (FTO), opens up broad prospects for applications in optoelectronic devices. Thus, AZO thin films are widely used as transparent electrodes [1], in solar cells [2], as photodetectors of UV radiation [3], for data recording and encryption [4]. For these applications, the resistivity of AZO films must be less than $10^{-3}$ Ω cm and visible transmittance should be over 85%. These parameters were previously achieved by using complex and expensive vacuum techniques. Therefore, there is an increasing interest in developing the AZO films by the low-cost non-vacuum deposition method, such as sol-gel. However, the resistivity of the sol-gel

developed AZO films is typically about $10^{-4}$ Ω cm, and the required electrical conductivity has not been achieved for these films. In fact, AZO films are known to contain extended defects, such as inter-grain voids, gaps, oxygen vacancies and grain boundaries. These defects are free carrier scattering centers and decrease the carrier lifetime that led to drawback the carrier mobility and low electrical conductivity.

Herein, we investigate the possibilities of precise laser-induced modifications of the composite structure, which is an AZO matrix with embedded silver nanoparticles. In the articles [5] it was shown that by varying the heat treatment conditions of annealing of sol-gel prepared AZO films with silver nanoparticles, one can change their structure and optical properties in a controlled way. This opens the opportunities for their application in optoelectronics. For example, to realize the Purcell effect in LED structures [6], to increase the efficiency of photovoltaics [7], photodetection [8]. The laser heat treatment is much more localized and acts directly on the electrical and optical characteristics of AZO films with silver nanoparticles. Previously, pulsed excimer lasers were already used for these purposes with temperature regimes of local heating of the film from 800–1200 K [9]. However, several drawbacks were revealed in these studies. Firstly, the laser radiation wavelength in the deep UV range and the short pulse duration (4-10 ns) leads to the accumulation of excessively absorbed energy in the film. This may be a reason for thin film destruction due to high tension. Secondly, the low repetition rate of excimer laser pulses prevents efficient laser scanning, which is crucial for applications. Moreover, excimer lasers typically lead to excessively strong heating of silver nanoparticles with their subsequent escape from AZO. For example, silver nanoparticles after heating at 700° C can transit into quartz substrate below the film, as was shown in Ref. [10]. All these facts narrow the area of the optimal processing conditions. On the other hand, the complexity of an excimer laser operation, specific optics for beam focusing and the risk of human skin deep UV exposure significantly limit the use of excimer lasers in industry.

The aims of our work are to investigate induced local changes in the properties of AZO semiconductor thin films with Ag NPs under gentle CW visible laser irradiation with a wavelength far from the peak of the plasmon resonance of nanoparticles. Compared to the previously used pulsed lasers, our CW lasers allow thermal modification of the structure to be carried out more smoothly due to lower heating and cooling rates of the material. The operating modes range is wider here, and the modification process is easier to control. In turn, the use of a wavelength away from the peak maximum also allows a much more controlled laser processing. The closer the wavelength is to the maximum, the stronger the absorption of radiation on nanoparticles, due to which the processes of changing their size, concentration, shape, etc. occur more intensively. This leads to a change in the absorbance of the material and non-stationary heating processes, which

makes processing less controllable and well-studied on the example of $TiO_2$:Ag films [11]. The morphological and spectral characteristics of films before and after laser exposure were studied, a corresponding numerical model was developed, and a mechanism of film laser treatment was proposed.

## 2. Materials and Methods

Thin polycrystalline AZO thin films with Ag NPs (AZO:Ag) were obtained by using the sol-gel method [12]. The AZO films were created from the solution of zinc acetate and aluminum nitrate in ethylene glycol monomethyl ether with a concentration of 0.2 M. The percentage of Al in the films was 0.5 wt%. An AZO film was deposited onto a 1 mm thick fused silica substrate by centrifugation. To achieve film thickness h = 120 ± 5 nm the deposition of layers was repeated 10 times. After each deposition the sample was dried at 300°C for 5 minutes to evaporate the solvent. To obtain Ag NPs, a solution of silver nitrate in ethylene glycol monomethyl ether with a concentration of 0.03 M was created. A layer of Ag NPs inside the AZO film was obtained by sequential deposition of 5 layers of AZO and silver solutions.

Because the initial grain size in the film was only 3-5 nm, the final stage of obtaining a polycrystalline AZO film with Ag NPs was the stage of heat treatment (HT) of the layers in the muffle furnace. HT was performed in air at a temperature of 570°C for 15 minutes and provided crystallization and coarsening of AZO grains and Ag NPs to a size of 15-25 nm. Processing in the furnace did not lead to significant changes in h, which varied within the error. In turn, Ag atoms/ions were migrating through the thickness of the AZO matrix forming Ag NPs in the initial layer. The described sample preparation conditions provided the following advantages

(i) stabilization of the characteristics of the film during long-term storage in air;

(ii) improving the adhesion of the film to the substrate;

(iii) uniform distribution of nanoparticles over the film thickness;

(iv) partial absorption of the incident laser radiation by the film matrix for its uniform heating during exposure;

(v) high absorption of incident radiation by nanoparticles in the film to activate the processes of their modification during irradiation.

The semiconductor CWV laser LSR405CP-2W with $\lambda$ = 405 nm was used for film processing (Fig. 1). The initial $TEM_{10}$ beam after the diaphragm had a square cross section of 1.5x1.5 mm and uniform intensity distribution. Laser radiation was focused by a 60x objective (NA = 0.85) with focal length F = 200 μm into the beam with radius $r_0$ = 1.5 μm. A three-coordinate movable table provided scanning over the sample surface. During the tracks recording the incident power on the film equaled P = 20 mW and P = 24 mW, which corresponded to the power density

$I_0$ = 0.89 MW/cm$^2$ and $I_0$ = 1.07 MW/cm$^2$. The scanning velocity during the recording tracks was $V_{sc}$ = 100 μm/s and $V_{sc}$ = 50 μm/s.

The wavelength and other parameters of laser radiation were chosen based on the following considerations

(i) the absence of resonant absorption on nanoparticles, i.e. the radiation wavelength is not equal to the plasmon resonance wavelength ($\lambda_{laser} \neq \lambda_{plasm}$);

(ii) the absorption of radiation on nanoparticles should be much higher than the reflection, i.e. A >> R;

(iii) power density and exposure time t (t = d/υ, where d is the laser spot diameter, υ is the scanning speed) should provide a change in the size and concentration of nanoparticles in the film and modification of the matrix structure without evaporation and destruction.

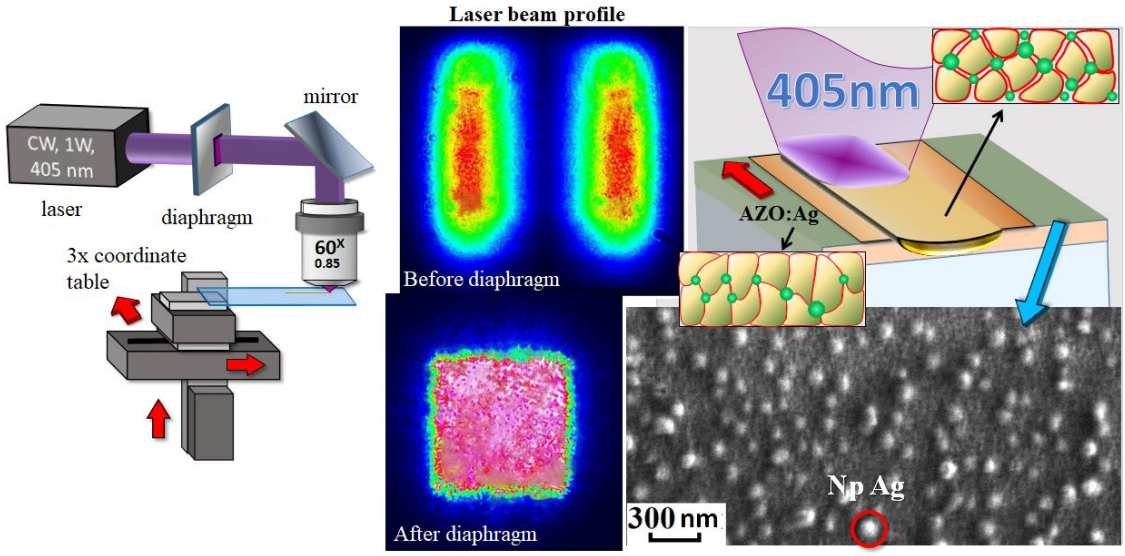


**Fig. 1.** (a) Experimental setup scheme for laser modification of AZO: Ag thin films in the matrix crystallization regime with growth / decomposition of Ag NPs; (b) original film SEM image.

After laser exposure, the sample surface was studied using an optical microscope, Carl Zeiss Axio Imager A1M in the reflected and transmitted light, in the bright and dark field. The morphology of the film relief was studied using a scanning probe microscope (SPM) NANOEDUCATOR and a scanning electron microscope (SEM). Spectral characteristics of the films in the spectral range from 200 nm to 1100 nm were studied using the SF-56 spectrophotometer. The optical characteristics of the treated areas were investigated in the spectral range from 330 nm to 800 nm using a microscope-spectrophotometer MSFU-K with a photometric area of 2.5 μm.

## 3. Results and Discussion

### 3.1 Optical constants of initial material

Spectral transmission ($T_{meas}$) and reflection ($R_{meas}$) of non-polarized light at normal incidence were measured (Fig. 2) with instrumental error 2-3%. $T_{meas}$ spectra of AZO:Ag shows the plasmon resonance peak with a minimum near 475 nm (green curve), which after HT shifted to 610 nm (orange curve). This peak is distinctive for Ag NPs. The shift of the peak was due to a change in the size of nanoparticles. As a result of heat treatment in an oven, the diameter of nanoparticles increased from 20–30 nm to 50–60. The 355 nm peak is distinctive for samples after HT in the furnace. This peak is located at the edge of the AZO matrix fundamental absorption. It indicates the incorporation of Al atoms into the ZnO matrix and the formation of the corresponding crystals [13] leading to a decrease in the bandgap [14]. In $R_{meas}$ spectra, there is a similar plasmon peak near 487 nm, which shifted to 790 nm after HT. The HT of AZO:Ag films led to a decrease in transmission and an increase in reflection indirectly indicating metallization due to the formation and coarsening of Ag NPs, as well as compaction of the matrix itself. Another notable peak near 1030 nm is distinctive for all samples in both the transmission and reflection spectra.

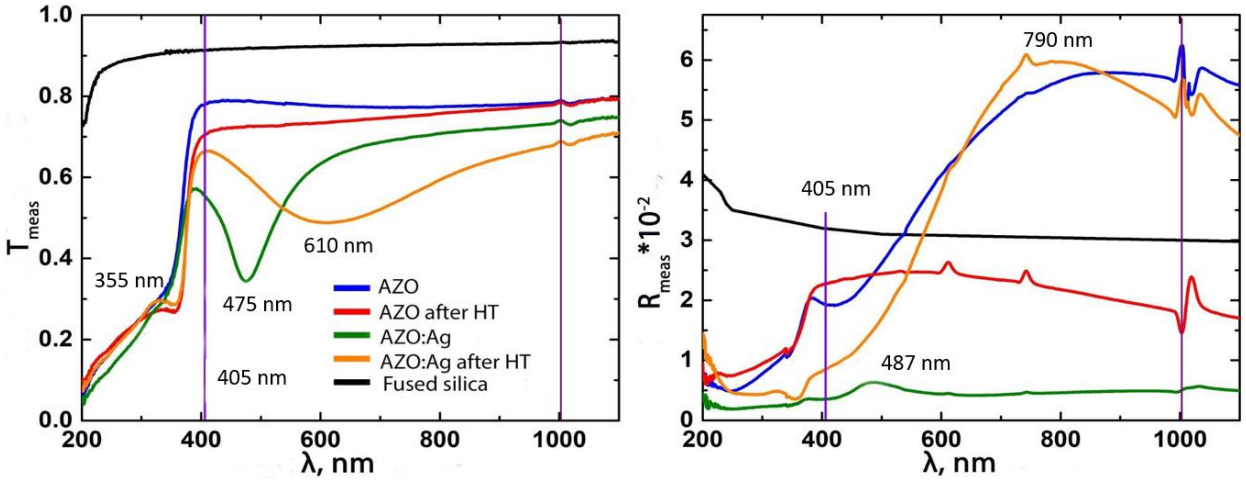


**Fig. 2.** Transmission (left) and reflection (right) of AZO films without HT (blue curve) and after HT in the furnace (red curve), as well as AZO:Ag without HT (green curve) and after HT in the furnace (orange curve).

Optical constants of the films were calculated by using numerical method [15]. The extinction $k_f$ was calculated according to the spectral characteristics of $T_{meas}$ and $R_{meas}$ (Fig. 3). Additionally, in Fig. 3 was shown the calculation error. It was high in the spectral range 200 - 350 nm, which is characteristic of low transmission in the region of fundamental absorption of the film matrix.

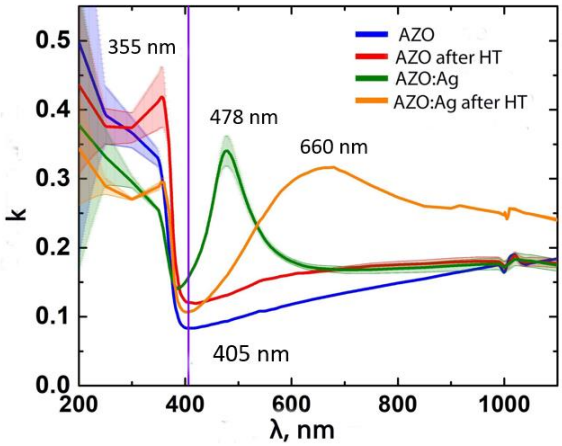


**Fig. 3.** Extinction of AZO and AZO: Ag films without HT and after HT in the furnace. Colored areas around the curves correspond to the error bars.

The $k_f$ curves clearly show that the HT stage did not lead to a significant change in the extinction of the AZO matrix (Fig. 3). The addition of silver to AZO/Ag films led to an abrupt increase in extinction near 478 nm before HT. After HT its value increased significantly in the spectral range of 500 - 1100 nm. This indicates an increase in the volume fraction of the second phase in the form of Ag NPs after HT.

The bandgap energy Eg in the AZO and AZO:Ag systems was determined by the equation $\alpha h\nu=B(h\nu-Eg)\gamma$ [16], where $\alpha = 2\pi kf(\lambda)/\lambda$ is the absorption index; hν is the energy of the incident photons; B is a constant that depends on the concentration and mobility of free charge carriers in the material and denotes the length of the bandgap; γ is the gain for all possible transitions in the electronic system. The coefficient γ corresponds to 1/2 for direct allowed, 3/2 for direct forbidden, 2 for indirect allowed and 3 for indirect forbidden transitions [17]. Concerning the parameters, $\gamma = 1/2$ is typical for crystalline solids and $\gamma = 2$ for amorphous materials. Based on the kf data, the corresponding dependences were plotted (Fig. 4). The energy of direct allowed transitions ($\gamma = 1/2$) was: 1.9 eV for AZO, 1.55 eV for AZO after HT, 1.22 eV for AZO:Ag, and 1.45 eV for AZO:Ag after HT. The presence of Ag in the film led to a decrease in the transition energy. However, after HT in the furnace, transition energy increased again. The energy of indirect allowed transitions ($\gamma = 2$) increased to the following values: 3.29 eV for AZO, 3.26 eV for AZO after HT in the furnace, 3.25 eV for AZO:Ag, and 3.27 eV for AZO:Ag after HT. For AZO, the observed decrease in the transition energy can be associated with an increase of the ZnO crystals after annealing. The assumption of an increase in the size of crystals is based on the results of the work [18]. The larger crystal size leads to the lower quantization level, and respectively to the lower energy values. In the case of AZO:Ag, heat treatment commonly leads to an increase in the number of free carriers, which in turn results in an increase in the transition energies.

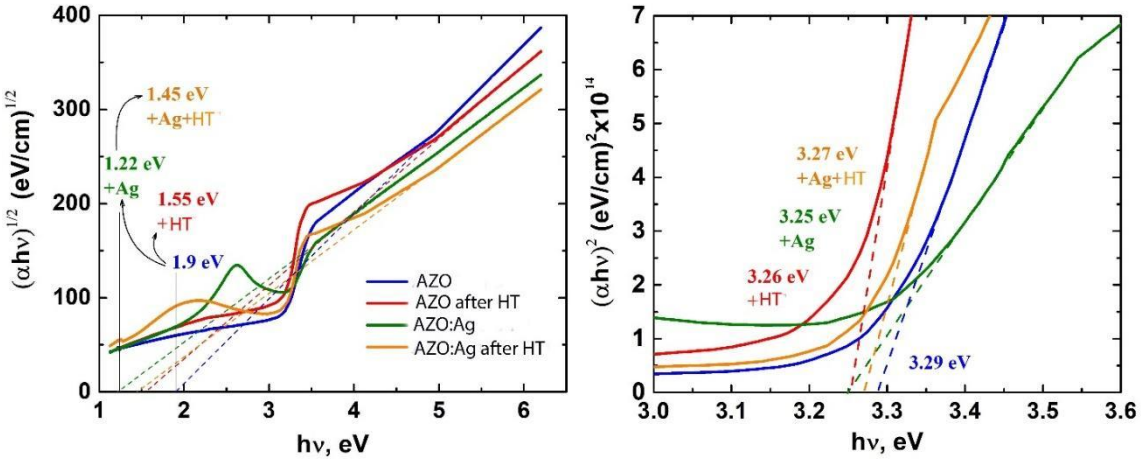


**Fig. 4.** Dependencies $(\alpha h\nu)^{1/2}$ (right) and $(\alpha h\nu)^2$ (left) on the photon energy of incident radiation *hv* for AZO and AZO:Ag films.

### 3.2 Laser treatment

For laser treatment, AZO:Ag samples obtained after HT were used. The wavelength of laser radiation (405 nm) is at the edge of the fundamental absorption of the AZO matrix, and is weakly absorbed by such films without NPs. The addition of Ag to the AZO film stage led to an increase in absorption from 0.20 to 0.44. After HT in the furnace, the presence of Ag NPs in the film changed the absorption from 0.28 to 0.35. Thus, the HT led to an increase in absorption up to 0.11 with Ag NPs and by 0.08 without them. The absorption of NPs made it possible to reduce the intensity of laser power needed for film modification. As a result of laser treatment, the morphological properties of the film were modified.

The optical images of the recorded tracks show the local change in optical characteristics after laser treatment. In the transmitted light (Tl) mode (fig. 5a) one can see the brightening of the film, while darkening is observed in the reflected light (Rl) mode (Fig. 5b). Neither before laser treatment nor after the films did not exhibit any anisotropic properties.

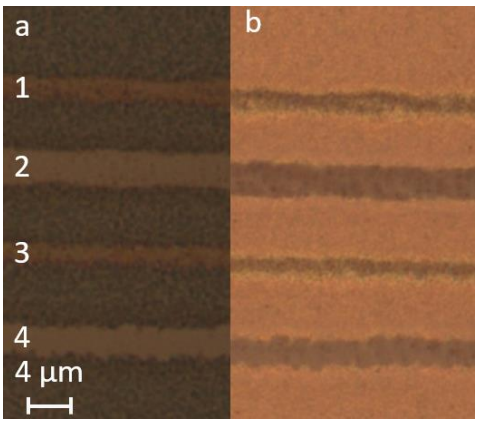

**Fig. 5.** Optical images of the recorded tracks. 1 – $V_{sc}$ =50 μm/s, $I_0$=0.89 MW/cm$^2$; 2 – 50 μm/s, 1.07 MW/cm$^2$; 3 – 100 μm/s, 0.89 MW/cm$^2$; 4 – 100 μm/s, 1.07 MW/cm$^2$; (a) Tl, (b) Rl.

To investigate morphological modifications of the film before and after laser treatment, scanning electron microscopy was performed. In the SEM image the modified regions are darker than the original film, which indicates an increase in the film density (Fig. 6a). SEM image with higher magnification (fig. 6b) also show that the AZO matrix was heated to the softening temperature with the activation of viscous flow along the track. High speeds of heating and cooling led to the formation of cavitation pores, as well as to the decomposition of large NPs into smaller ones. The study of the sample relief using the SPM showed that the relief shrank by 50 – 70 nm after laser treatment. (Fig. 6c).

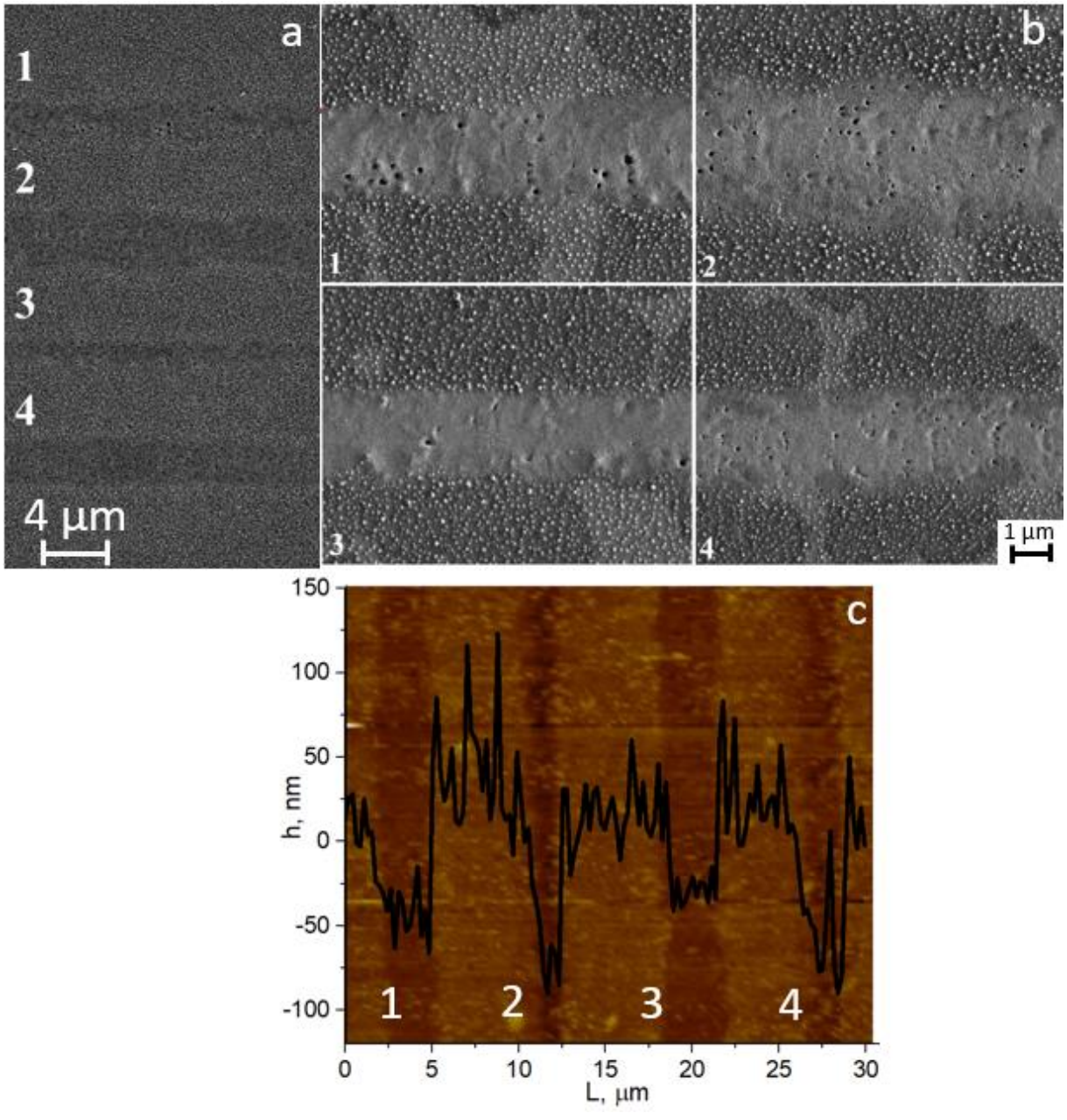

**Fig. 6.** (a) SEM images 1 – $V_{sc}$ = 50 μm/s, $I_0$ = 0.89 MW/cm$^2$; 2 – 50 μm/s, 1.07 MW/cm$^2$; 3 – 100 μm/s, 0.89 MW/cm$^2$; 4 – 100 μm/s, 1.07 MW/cm$^2$. (b) SEM images with higher magnification. (c) 2D image (top view) of the relief obtained with the SPM. The y-axis (h, nm) corresponds to the relief depth.

Interestingly, the film showed a polycrystalline structure under more precise investigation (Fig. 7). The structure consisted of AZO grains about 20 nm in size, separated by dark voids and amorphous material 10 nm size. The figure also shows a histogram of the Ag NPs distribution by diameter over the area of 1.5x1.5 μm$^2$. As a first approximation, it was assumed that all NPs are spherical. The diameter of Ag NPs varied from 50 to 100 nm. Most NPs had a diameter of about 65 nm.

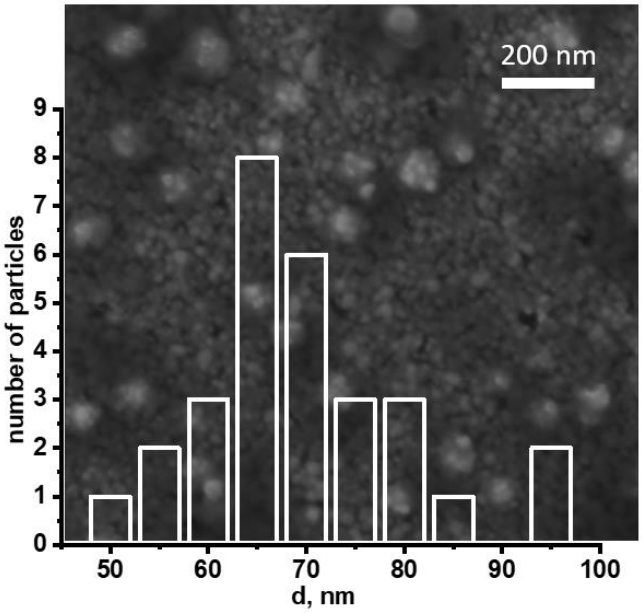


**Fig. 7.** SEM images of the original film and a histogram of Ag NPs size distribution by diametral size.

SEM images are shown in Fig. 8. The result of laser treatment is similar to the pulsed laser recrystallization with excimer laser [9]. Recrystallization of such films occurs when a certain temperature ($T_{cr}$) is reached. According to [9], the temperatures required for this process should be higher than 75% of the melting point ($T_m$). For AZO without NPs, Tm ≈ 1127 °C, hence $T_{cr}$ ≈ 777 °C. Under the laser radiation thermal energy increases, individual grains melt and combine into crystallites with the following rapid solidification. In this experiment recrystallization was achieved due to the presence of Ag NPs in the film, they increased

the absorption of laser radiation. After laser treatment NPs were distributed within crystallites, missing between them. The small dark voids in the original film disappeared after laser treatment. The diameter of the formed crystallites varied from 20 to 120 nm.

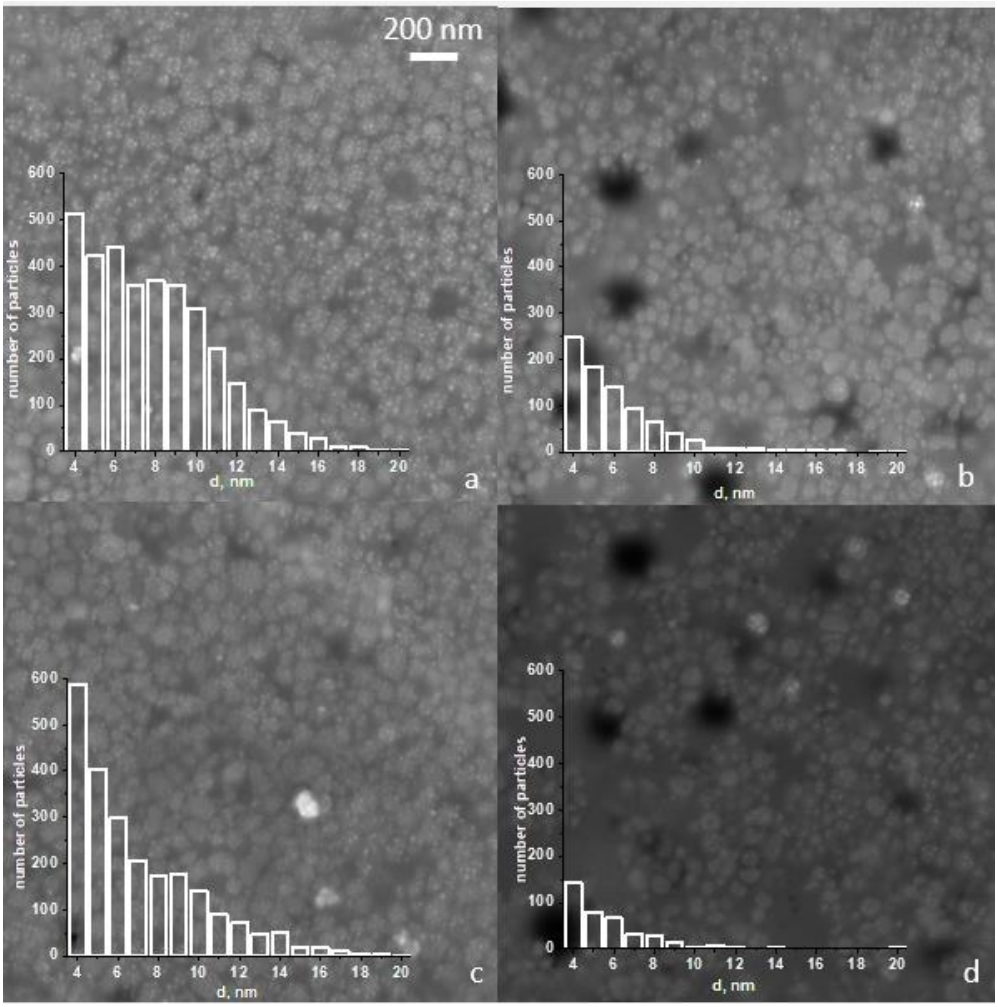


**Fig. 8.** SEM images of tracks. a) $V_{sc}$ = 100 μm/s, $I_0$ = 1.07 MW/cm$^2$; b) 100 μm/s, 0.89 MW/cm$^2$; c) 50 μm/s, 1.07 MW/cm$^2$; d) 50 μm/s, 0.89 MW/cm$^2$.

Fig. 8 shows histograms of NPs size distribution inside the tracks. For all regimes, the sizes of NPs remain the same: about 10 nm diameter or less. The highest concentration of NPs of all sizes in the track section 1.5x1.5 μm$^2$ was observed at $I_0$=1.07 MW/cm$^2$: 3400 and 2250 for $V_{sc}$ =100 μm/s and $V_{sc}$ =50 μm/s, respectively. The concentrations for $I_0$=0.89 MW/cm$^2$ were 400 and 800 for 100 μm/s and 50 μm/s, respectively. At the same time, in the tracks recorded at $I_0$=0.89 MW/cm$^2$, large non-crystallized regions without NPs were observed. This can be explained by the lower temperature established during laser exposure with $I_0$=0.89 MW/cm$^2$ (see Supplementary).

The proportion of such regions in the track area was 0.18 and 0.22 for $V_{sc}$ =100 μm/s and $V_{sc}$ =50 μm/s, respectively. However, the lowest proportion was also observed at the highest temperature.

Transmission and reflection spectra are shown in Fig. 9. $T_{meas}$ curves at 0.89 MW/cm$^2$ (blue and orange curves) are similar to the spectra of the AZO:Ag films without HT (Fig. 2 a, green curve) due to plasmon peaks of silver particles near the UV region. The intensity of the peak minimum in the transmission spectra are less than for the initial film: 0.39 for the initial AZO:Ag (dark curve), 0.52 and 0.57 at 100 μm/s and 50 μm/s, respectively. An increase in the radiation intensity to $I_0$=1.07 MW/cm$^2$ led to a reverse shift of the plasmon resonance peaks to the IR region, with the minimum near 0.7. Decrease in the scanning velocity from $V_{sc}$ =100 to $V_{sc}$ =50 μm/s led to a shift in the minimum of transmission spectra to IR by 22–25 nm, irrespective of the radiation intensity. For both regimes the brightening of the film occurred. Its transmission after processing increased. The highest transmission was obtained at $V_{sc}$ =100 μm/s and $I_0$=1.07 MW/cm$^2$.

For the reflection spectra there were also peaks with a maximum near 650-660 nm. Moreover, the intensity of these peaks, as well as the average reflection for the treated areas, was lower than that of the original film. An increase in transmission and a decrease in reflection attributed to a decrease in the film thickness. In addition, the recrystallization of the film caused these changes through reducing the number of defects in the AZO structure. In the polycrystalline film they were additional centers of scattering and absorption of radiation. A decrease in the concentration of NPs can lead to similar effects. A small peak at 400 nm in the transmission spectra is distinctive to the edge of fundamental absorption of the film. It shifts by 10–15 nm to the UV region after laser treatment and remains permanent irrespective to the influence regime.

The obtained optical characteristics were used to calculate the extinction and estimate the energy of the bandgap for indirect allowed transitions. The action of laser radiation led to an increase in the bandgap of the film from 3.27 eV to 3.32 - 3.36 eV (Fig. 9d), so-called blue shift. This shift is associated with an increase in the concentration of free electrons in the material. After generation, new charge carriers fill the lower levels of the conduction band of the AZO:Ag film. That leads to the fact that electrons from the semiconductor valence band need to spend more energy to overcome the bandgap, which requires the action of photons with a shorter wavelength. An increase in the concentration of free electrons is associated with laser activation of Al ions, as well as with an increase of oxygen vacancies in the AZO matrix, which are electron donors [19]. Moreover, Ag NPs were additional sources of charge carriers. Ag electrons under the irradiation could move to the AZO conduction band.

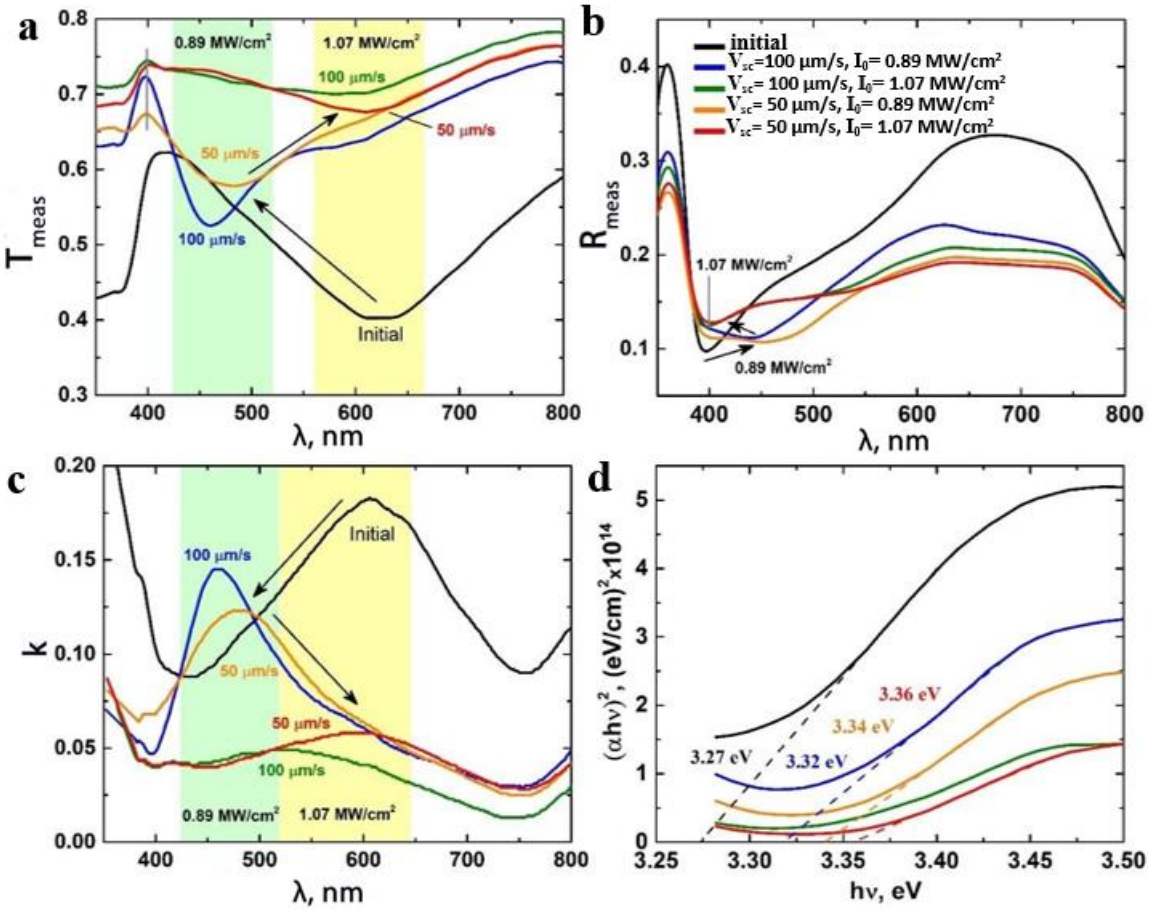


**Fig. 9.** Transmission (a), reflection (b), extinction (c), and curve $(\alpha h\nu)^2$ (d) for the original film (black) and recorded tracks $V_{sc}$=100 μm/s, $I_0$=0.89 MW/cm$^2$ (blue); $V_{sc}$=100 μm/s, $I_0$=1.07 MW/cm$^2$ (green); $V_{sc}$=50 μm/s, $I_0$=0.89 MW/cm$^2$ (orange); $V_{sc}$=50 μm/s, $I_0$=1.07 MW/cm$^2$ (red).

### 3.3 Discussion over photothermal structure modification

The mechanism of laser modification of the film is associated with thermal processes caused by the heat source acting on both the film matrix and NPs. The formation of the heat source in the laser beam focusing area is associated with the partial absorption of radiation on the matrix and NPs. The substrate under the film did not absorb laser radiation but was heated due to heat transfer from the heated film. In the laser radiation absorption area, an abrupt heating of the material occurred. With a temperature of 640 – 776 °C at the epicenter and a heat source size of 3 – 6 μm, the temperature gradient dT/dr reached 192 – 213 °C/μm. The heating rate was $(8 – 26)\cdot10^3$ °C/s when the laser spot moved at a velocity of 50 – 100 μm/s. Heating from room temperature to the maximum temperature proceeded in 0.5 – 1.0 s. That led to extreme conditions for heating the film with various stages of its modification. All data of the heat source was difficult to measure in the experiment, so it was modeled based on the obtained

information about the modified regions and thermophysical characteristics of the film (see supplementary).

In the beginning of laser treatment Ag NPs decomposed into atoms, ions, and monomers. They concentrated at the boundaries of AZO crystals (Fig. N, I). Next, there was a diffusion mass transfer of Ag in the form of monomers along the temperature gradient from the center of the film to its surface and to the film-substrate interface, where the temperature was lower (Fig. N, II). Simultaneously with the mass transfer of Ag, the AZO matrix thermally compacted and recrystallized. Assumably, at this moment the absorption capacity of the film decreased due to the destruction of large Ag NPs. After that, the heat front began to spread outside the film, that led to the softening of the substrate under the exposed area due to heat transfer from the heated film to the glass substrate. Due to this phenomenon, the outflow of Ag monomers from the film to the substrate sharply increased. When the heat source was removed, Ag nanoclusters grew on the film surface during its cooling (Fig. N, III). In the softened substrate Ag monomers began to agglomerate forming Ag NPs under the film (Fig. N, IV). The growth of Ag NPs in the substrate ended only when the heat source was removed, the temperature dropped, and the glass solidified. Since the film modification occurred due to thermal action of laser radiation, such a mechanism can be called photothermal.

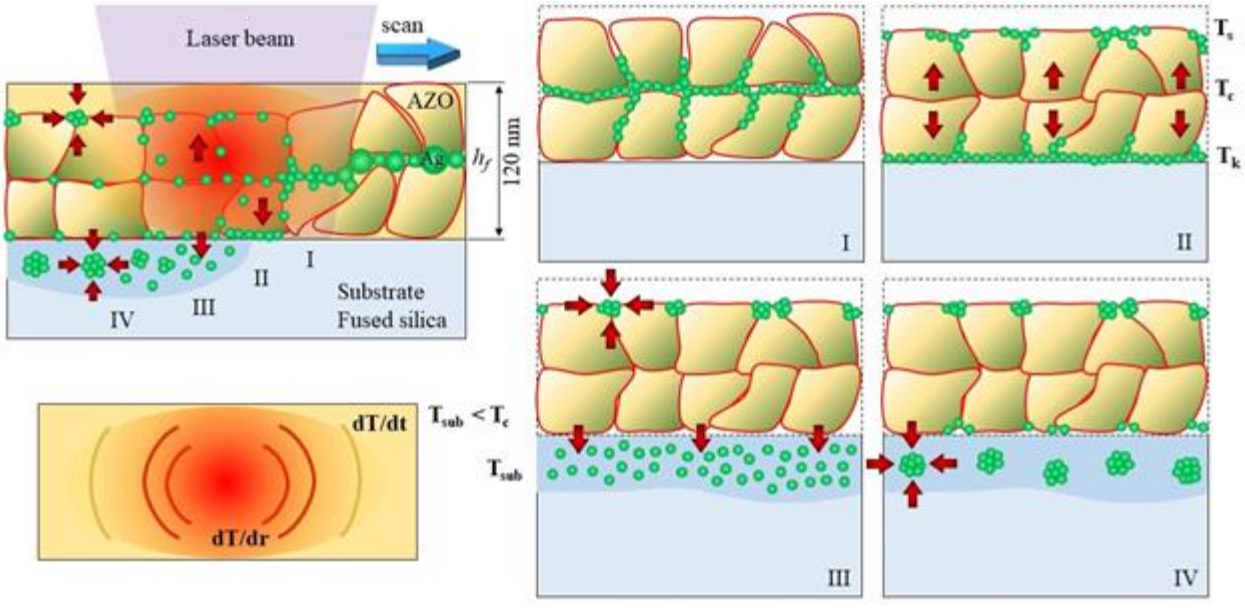


**Fig. 11.** The scheme of AZO:Ag film photothermal modification with the following stages: I. Decomposition of Ag NPs into monomers; II. mass transfer of Ag monomers from the center of the film to the surface and to the film-substrate interface; III. the outflow of Ag monomers from the film to the substrate during its softening, as well as the growth of Ag nanoclusters on the film surface; IV. agglomeration of Ag monomers and growth of NPs in the substrate.

## 4. Conclusion

Under the influence of CW radiation with a wavelength of 405 nm, the structure of AlZnO films with silver nanoparticles on a glass substrate was recrystallized. The treatment was possible due to the presence of silver nanoparticles, which increased the absorption efficiency. As a result of recrystallization, smaller crystallites were combined into larger ones, about 80 nm in size. Initial nanoparticles with diameters of about 65 nm were concentrated within individual crystallites after laser treatment. The particle diameter decreased down to 10 nm or less. At $I_0$=0.89 MW/cm$^2$ at both scanning velocity, the maximum of the plasmon resonance peak in the transmission and extinction spectra was shifted to a wavelength of 450 nm; at $I_0$=1.07 MW/cm$^2$, a significant decrease in the peak intensity was obtained. The study of the bandgap showed that it rose up from 3.27 eV to 3.36 eV due to an increase in the concentration of charge carriers after exposure. A photothermal mechanism for film modification was proposed, the recrystallization of AZO and a decrease in the size of nanoparticles occurred due to the thermal effect of laser radiation. The results of this paper can be used for optical recording of information and its encryption [4], in the field of photodetection [8] and in LED [6].

## Supplementary

To estimate the range and gradient of film temperatures in the region of laser action, as well as the heating rate, the heat source was modeled. In the region of a laser spot with a rectangular cross section, the laser radiation was partially absorbed, and a heat source was formed. To describe the heat source, a model of heating by CW laser radiation in the scanning mode was used [20]. The following approximations were used:

1. Laser radiation was absorbed only by the film and was not absorbed by the substrate, the transmission of the film at a wavelength of 405 nm (see fig. 2) changed from $T_{AZO}$ = 0.705 to $T_{AZO: Ag}$ = 0.663, and the reflection from $R_{AZO}$ = 0.022 to $R_{AZO: Ag}$ = 0.008, therefore, its absorption capacity was $A_{AZO}$ = 0.273 and $A_{AZO: Ag}$ = 0.329.
2. During the treatment, NPs were destroyed, which led to a decrease in the absorption of the film from $A_{AZO: Ag}$ to $A_{AZO}$. A depended on the time of thermal action τ in the XY plane as follows:

$$A(\tau, x, y) = A_{AZO:Ag}\left[1 - 0.085\exp\left(-4\frac{y^2}{y_0^2}\right)erfc\left(2\frac{x}{y_0} + \frac{\upsilon r_{hs}}{4a_f}\tau\right)\right], \quad (1)$$

$$\tau = \frac{1}{0.52r_{hs}}\sqrt{a_f\frac{2r_{hs}}{\upsilon}}, \quad (2)$$

there $2y_0$ – cross-sectional dimension of the modified track, $a_f$ = 1.92 mm$^2$/s – thermal diffusivity of the film, υ = 100, 50 μm/s – scanning velocity, $r_{hs}$ = 0.85 μm laser spot radius. For $q$ = 0.89 MW/cm$^2$ $y_0$ = 0.9 μm, for $q$ = 1.07 MW/cm$^2$ $y_0$ = 1.5 μm.

3. Laser spot shape corresponded to a square with a side $2r_{hs}$ = 1.7 μm.
4. Heat outflow from the heated area occurred into the air and into the substrate (fused silica) at the following thermal diffusivity values: $a_{\text{air}}$ = 0.2107 mm$^2$/s and $a_{\text{sub}}$ = 0.5956 mm$^2$/s.
5. Heat transfer at the film-air and film-substrate boundaries was determined by the following coefficients: $\alpha_{FA}$ = 25.15 W/m$^2$K and $\alpha_{FS}$ = 100.9 W/m$^2$K.
6. Thermal conductivity, heat capacity, and density of the film during laser exposure were constant.

Absorbed energy flux was set by the following equations for the environment, the film, and the substrate below it:

$$Q(z)=\begin{bmatrix}\alpha_{FA}\left(T_{\max}-T_0\right)\pi r_{hs}^2, & z<-0.5h_f,\\ \dfrac{A(\tau_s,x,y)P-\left(\alpha_{FA}+\alpha_{FS}\right)\left(T_{\max}-T_0\right)\pi r_{hs}^2}{128kR}, & z\le 0.5h_f\wedge z\ge -0.5h_f,\\ \alpha_{FS}\left(T_{\max}-T_0\right)\pi r_{hs}^2, & z<0.5h_f,\end{bmatrix}, \quad (3)$$

there $h_f$ – film thickness, $T_0$ = 273 K, $T_{max}$ – maximum temperature, $k$ = 5.4 W/mK – thermal conductivity, $P$ = 20 and 24 mW – incident power. Radius $R$ is the average size of the heat source, equal to

$$R=\sqrt[3]{r_{hs}^2h_f}. \quad (4)$$

The temperature distribution in the affected area was described as the heat inflow and outflow:

$$\begin{bmatrix}dT_x(x,\tau)\\ dT_y(y,\tau)\\ dT_z(z,\tau)\end{bmatrix}=\begin{bmatrix}erfc\left(\dfrac{x-r_{hs}}{R\tau}+\dfrac{\upsilon R}{4a}\tau\right)-erfc\left(\dfrac{x+r_{hs}}{R\tau}+\dfrac{\upsilon R}{4a}\tau\right)\\ erfc\left(\dfrac{y-r_{hs}}{R\tau}\right)-erfc\left(\dfrac{y+r_{hs}}{R\tau}\right)\\ erfc\left(\dfrac{z-0.5h_f}{R\tau}\right)-erfc\left(\dfrac{z+0.5h_f}{R\tau}\right)\end{bmatrix}, \quad (5)$$

there a – thermal diffusivity of air ($a_{air}$), film ($a_f$), and substrate ($a_{sub}$):

$$a=\begin{bmatrix}a_{air}, & z<-0.5h_f,\\ a_f, & z\le 0.5h_f\wedge z\ge -0.5h_f,\\ a_{sub}, & z<0.5h_f.\end{bmatrix} \quad (6)$$

Temperature distribution:

$$T(x,y,z) = Q(z)\int_0^t dT_x(x,\tau)\,dT_y(y,\tau)\,dT_z(z,\tau)\,\tau\,d\tau, \tag{7}$$

there $t$ – effective heating time of the film $t = R^{-1}(2ar_{hs}/\upsilon)^{0.5}$.

Maximum temperatures and the heat source shape in the laser action zone were estimated (fig. 01). After reaching the maximum temperature, the absorption capacity of the film dropped. This led to a decrease in temperature already at the center of the laser spot. The maximum temperature at the center of the laser spot could reach 640–776 °C, with heating rate (8 – 26) $*10^3$ °C/s. Due to the small size of the laser spot, the temperature gradient could reach values 192 – 213 °C/ μm. Such a small size of the laser spot and the localization of the heat source ensured high heating temperatures at low radiation power, sufficient for melting the matrix and modifying NPs in it.

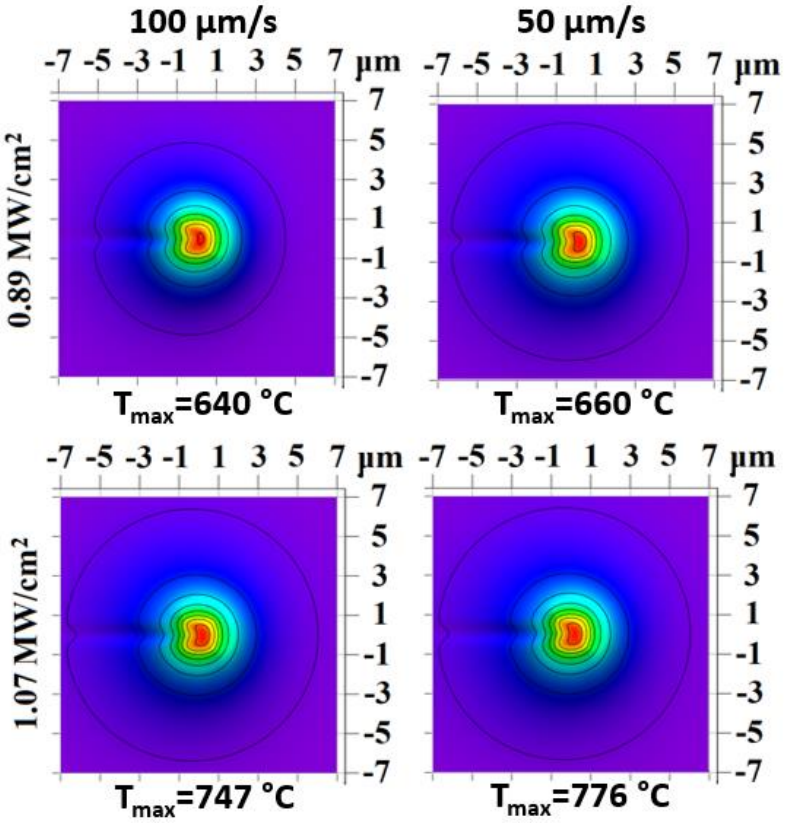


**Fig. 01.** shape of the heat source depending on the radiation intensity and scanning velocity.


## Funding

This research was funded by the grant of the Russian Science Foundation (project No. 19-79-10208).

## Acknowledgments

SEM measurements were done on the base of the Interdisciplinary Resource Center for Nanotechnology, Research Park, St. Petersburg State University.

## Declaration of Competing Interest

The authors declare that they have no known competing financial interests or personal relationships that could have appeared to influence the work reported in this paper.

## CRediT authorship contribution statement

**Maksim M. Sergeev:** Conceptualization, Methodology, Writing - Original Draft, Funding acquisition, Supervision. **Vladislav R. Gresko:** Investigation, Visualization, Validation, Writing - Original Draft. **Yaroslava M. Andreeva:** Writing - Review & Editing, Validation. **Lilia A. Sokura:** Resources. **Elena V. Shirshneva-Vaschenko:** Resources. **Tatiana E. Itina:** Supervision of the modeling-Writing - Review & Editing, Validation. **Georgii V. Varygin:** SEM investigation.

## References


[1] Machda F, Ogawa T, Okumura H, Ishihara KN. Damp-heat durability comparison of Al-doped ZnO transparent electrodes deposited at low temperatures on glass and PI-tape/PC substrates. Ceramics International 2020;46:16178–84. https://doi.org/10.1016/j.ceramint.2020.03.173.

[2] Pugazhendhi K, Praveen B, Sharmila DJ, Sahaya Selva Mary J, Naveen Kumar P, Bharathilenin V, et al. Plasmonic TiO2/Al@ZnO nanocomposite-based novel dye-sensitized solar cell with 11.4% power conversion efficiency. Solar Energy 2021;215:443–50. https://doi.org/10.1016/j.solener.2020.12.031.

[3] Marques AC, Faria J, Perdigão P, Faustino BMM, Ritasalo R, Costabello K, et al. Stability under humidity, UV-light and bending of AZO films deposited by ALD on Kapton. Scientific Reports 2019;9. https://doi.org/10.1038/s41598-019-54451-0.

[4] Castro-Chacón JH, Torres-Torres C, Khomenko A v., García-Zárate MA, Trejo-Valdez M, Martínez-Gutiérrez H, et al. Encryption of nonlinear optical signals in ZnO:Al thin films by ultrashort laser pulses. Journal of Modern Optics 2017;64:601–8. https://doi.org/10.1080/09500340.2016.1253880.

[5] Shirshneva-Vaschenko E v., Sokura LA, Baidakova M v., Yagovkina MA, Snezhnaia ZG, Shirshnev PS, et al. Study of the influence of the ZnO:Al polycrystalline film morphology on the silver nanoparticles formation. Journal of Physics: Conference Series, vol. 1400, Institute of Physics Publishing; 2019. https://doi.org/10.1088/1742-6596/1400/5/055026.

[6] Koenderink AF. On the use of Purcell factors for plasmon antennas 2010. https://doi.org/10.1364/OL.35.004208.

[7] Nasser H, Saleh ZM, Özkol E, Günoven M, Bek A, Turan R. Fabrication of Ag Nanoparticles Embedded in Al:ZnO as Potential Light-Trapping Plasmonic Interface for Thin Film Solar Cells. Plasmonics 2013;8. https://doi.org/10.1007/s11468-013-9562-6.

[8] Tzeng S-K, Hon M-H, Leu I-C. Improving the Performance of a Zinc Oxide Nanowire Ultraviolet Photodetector by Adding Silver Nanoparticles. Journal of The Electrochemical Society 2012;159. https://doi.org/10.1149/2.088204jes.

[9] Zhang MY, Cheng GJ. Highly conductive and transparent alumina-doped ZnO films processed by direct pulsed laser recrystallization at room temperature. Applied Physics Letters 2011;99. https://doi.org/10.1063/1.3622645.

[10] Sokura LA, Shirshneva-Vaschenko E v., Kirilenko DA, Snezhnaia ZG, Shirshnev PS, Romanov AE. Electron-microscopy study of ordered silver nanoparticles synthesized in a ZnO:Al polycrystalline film. Journal of Physics: Conference Series, vol. 1410, 2019. https://doi.org/10.1088/1742-6596/1410/1/012170.

[11] Ma H, Bakhti S, Rudenko A, Vocanson F, Slaughter DS, Destouches N, et al. Laser-Generated Ag Nanoparticles in Mesoporous TiO2 Films: Formation Processes and Modeling-Based Size Prediction. Journal of Physical Chemistry C 2019;123:25898–907. https://doi.org/10.1021/acs.jpcc.9b05561.

[12] Shirshneva-Vaschenko E v., Sokura LA, Shirshnev PS, Kirilenko DA, Snezhnaia ZG, Bauman DA, et al. Preparation of transparent N-ZnO:Al / p-CuAlCrO 2 heterojunction diode by sol-gel technology. Reviews on Advanced Materials Science 2018;57. https://doi.org/10.1515/rams-2018-0061.

[13] Al-Ghamdi AA, Al-Hartomy OA, el Okr M, Nawar AM, El-Gazzar S, El-Tantawy F, et al. Semiconducting properties of Al doped ZnO thin films. Spectrochimica Acta - Part A: Molecular and Biomolecular Spectroscopy 2014;131. https://doi.org/10.1016/j.saa.2014.04.020.

[14] Caglar M, Ilican S, Caglar Y, Yakuphanoglu F. The effects of Al doping on the optical constants of ZnO thin films prepared by spray pyrolysis method. Journal of Materials Science: Materials in Electronics, vol. 19, 2008. https://doi.org/10.1007/s10854-007-9386-2.

[15] Tomlin SG. Optical reflection and transmission formulae for thin films. Journal of Physics D: Applied Physics 1968;1. https://doi.org/10.1088/0022-3727/1/12/312.

[16] Abutalib MM, Rajeh A. Influence of ZnO/Ag nanoparticles doping on the structural, thermal, optical and electrical properties of PAM/PEO composite. Physica B: Condensed Matter 2020;578. https://doi.org/10.1016/j.physb.2019.411796.

[17] Aziz SB, Brza MA, Nofal MM, Abdulwahid RT, Hussen SA, Hussein AM, et al. A comprehensive review on optical properties of polymer electrolytes and composites. Materials 2020;13. https://doi.org/10.3390/MA13173675.

[18] Sokura LA, Shirshneva-Vaschenko E v., Kirilenko DA, Snezhnaia ZG, Shirshnev PS, Romanov AE. Electron-microscopy study of ordered silver nanoparticles synthesized in a ZnO:Al polycrystalline film. Journal of Physics: Conference Series, vol. 1410, Institute of Physics Publishing; 2019. https://doi.org/10.1088/1742-6596/1410/1/012170.

[19] Nian Q, Callahan M, Saei M, Look D, Efstathiadis H, Bailey J, et al. Large scale laser crystallization of solution-based alumina-doped zinc oxide (AZO) Nanoinks for highly transparent conductive electrode. Scientific Reports 2015;5. https://doi.org/10.1038/srep15517.

[20] Miyamoto I, Horn A, Gottmann J. Local melting of glass material and its application to direct fusion welding by Ps-laser pulses. Journal of Laser Micro Nanoengineering 2007;2. https://doi.org/10.2961/jlmn.2007.01.0002.